

Study of CP Violating Effects in Time Dependent $B^0(\bar{B}^0) \rightarrow D^{(*)\mp}\pi^\pm$ Decays

K. Abe,⁹ K. Abe,⁴⁴ N. Abe,⁴⁷ R. Abe,³⁰ T. Abe,⁹ I. Adachi,⁹ Byoung Sup Ahn,¹⁶
H. Aihara,⁴⁶ M. Akatsu,²³ M. Asai,¹⁰ Y. Asano,⁵¹ T. Aso,⁵⁰ V. Aulchenko,² T. Aushev,¹³
S. Bahinipati,⁵ A. M. Bakich,⁴¹ Y. Ban,³⁴ E. Banas,²⁸ S. Banerjee,⁴² A. Bay,¹⁹
I. Bedny,² P. K. Behera,⁵² I. Bizjak,¹⁴ A. Bondar,² A. Bozek,²⁸ M. Bračko,^{21, 14}
J. Brodzicka,²⁸ T. E. Browder,⁸ M.-C. Chang,²⁷ P. Chang,²⁷ Y. Chao,²⁷ K.-F. Chen,²⁷
B. G. Cheon,⁴⁰ R. Chistov,¹³ S.-K. Choi,⁷ Y. Choi,⁴⁰ Y. K. Choi,⁴⁰ M. Danilov,¹³
M. Dash,⁵³ E. A. Dodson,⁸ L. Y. Dong,¹¹ R. Dowd,²² J. Dragic,²² A. Drutskoy,¹³
S. Eidelman,² V. Eiges,¹³ Y. Enari,²³ D. Epifanov,² C. W. Everton,²² F. Fang,⁸ H. Fujii,⁹
C. Fukunaga,⁴⁸ N. Gabyshev,⁹ A. Garmash,^{2, 9} T. Gershon,⁹ G. Gokhroo,⁴² B. Golob,^{20, 14}
A. Gordon,²² M. Grosse Perdekamp,³⁶ H. Guler,⁸ R. Guo,²⁵ J. Haba,⁹ C. Hagner,⁵³
F. Handa,⁴⁵ K. Hara,³² T. Hara,³² Y. Harada,³⁰ N. C. Hastings,⁹ K. Hasuko,³⁶
H. Hayashii,²⁴ M. Hazumi,⁹ E. M. Heenan,²² I. Higuchi,⁴⁵ T. Higuchi,⁹ L. Hinz,¹⁹
T. Hojo,³² T. Hokuue,²³ Y. Hoshi,⁴⁴ K. Hoshina,⁴⁹ W.-S. Hou,²⁷ Y. B. Hsiung,^{27, *}
H.-C. Huang,²⁷ T. Igaki,²³ Y. Igarashi,⁹ T. Iijima,²³ K. Inami,²³ A. Ishikawa,²³ H. Ishino,⁴⁷
R. Itoh,⁹ M. Iwamoto,³ H. Iwasaki,⁹ M. Iwasaki,⁴⁶ Y. Iwasaki,⁹ H. K. Jang,³⁹ R. Kagan,¹³
H. Kakuno,⁴⁷ J. Kaneko,⁴⁷ J. H. Kang,⁵⁵ J. S. Kang,¹⁶ P. Kapusta,²⁸ M. Kataoka,²⁴
S. U. Kataoka,²⁴ N. Katayama,⁹ H. Kawai,³ H. Kawai,⁴⁶ Y. Kawakami,²³ N. Kawamura,¹
T. Kawasaki,³⁰ N. Kent,⁸ A. Kibayashi,⁴⁷ H. Kichimi,⁹ D. W. Kim,⁴⁰ Heejong Kim,⁵⁵
H. J. Kim,⁵⁵ H. O. Kim,⁴⁰ Hyunwoo Kim,¹⁶ J. H. Kim,⁴⁰ S. K. Kim,³⁹ T. H. Kim,⁵⁵
K. Kinoshita,⁵ S. Kobayashi,³⁷ P. Koppenburg,⁹ K. Korotushenko,³⁵ S. Korpar,^{21, 14}
P. Križan,^{20, 14} P. Krokovny,² R. Kulasiri,⁵ S. Kumar,³³ E. Kurihara,³ A. Kusaka,⁴⁶
A. Kuzmin,² Y.-J. Kwon,⁵⁵ J. S. Lange,^{6, 36} G. Leder,¹² S. H. Lee,³⁹ T. Lesiak,²⁸
J. Li,³⁸ A. Limosani,²² S.-W. Lin,²⁷ D. Liventsev,¹³ R.-S. Lu,²⁷ J. MacNaughton,¹²
G. Majumder,⁴² F. Mandl,¹² D. Marlow,³⁵ T. Matsubara,⁴⁶ T. Matsuishi,²³
H. Matsumoto,³⁰ S. Matsumoto,⁴ T. Matsumoto,⁴⁸ A. Matyja,²⁸ Y. Mikami,⁴⁵
W. Mitaroff,¹² K. Miyabayashi,²⁴ Y. Miyabayashi,²³ H. Miyake,³² H. Miyata,³⁰
L. C. Moffitt,²² D. Mohapatra,⁵³ G. R. Moloney,²² G. F. Moorhead,²² S. Mori,⁵¹ T. Mori,⁴⁷
J. Mueller,^{9, †} A. Murakami,³⁷ T. Nagamine,⁴⁵ Y. Nagasaka,¹⁰ T. Nakadaira,⁴⁶ E. Nakano,³¹
M. Nakao,⁹ H. Nakazawa,⁹ J. W. Nam,⁴⁰ S. Narita,⁴⁵ Z. Natkaniec,²⁸ K. Neichi,⁴⁴
S. Nishida,⁹ O. Nitoh,⁴⁹ S. Noguchi,²⁴ T. Nozaki,⁹ A. Ogawa,³⁶ S. Ogawa,⁴³ F. Ohno,⁴⁷
T. Ohshima,²³ T. Okabe,²³ S. Okuno,¹⁵ S. L. Olsen,⁸ Y. Onuki,³⁰ W. Ostrowicz,²⁸
H. Ozaki,⁹ P. Pakhlov,¹³ H. Palka,²⁸ C. W. Park,¹⁶ H. Park,¹⁸ K. S. Park,⁴⁰ N. Parslow,⁴¹
L. S. Peak,⁴¹ M. Pernicka,¹² J.-P. Perroud,¹⁹ M. Peters,⁸ L. E. Piilonen,⁵³ F. J. Ronga,¹⁹
N. Root,² M. Rozanska,²⁸ H. Sagawa,⁹ S. Saitoh,⁹ Y. Sakai,⁹ H. Sakamoto,¹⁷ H. Sakaue,³¹
T. R. Sarangi,⁵² M. Satapathy,⁵² A. Satpathy,^{9, 5} O. Schneider,¹⁹ S. Schrenk,⁵
J. Schümann,²⁷ C. Schwanda,^{9, 12} A. J. Schwartz,⁵ T. Seki,⁴⁸ S. Semenov,¹³ K. Senyo,²³
Y. Settai,⁴ R. Seuster,⁸ M. E. Sevior,²² T. Shibata,³⁰ H. Shibuya,⁴³ M. Shimoyama,²⁴
B. Shwartz,² V. Sidorov,² V. Siegle,³⁶ J. B. Singh,³³ N. Soni,³³ S. Stanič,^{51, †} M. Starič,¹⁴
A. Sugi,²³ A. Sugiyama,³⁷ K. Sumisawa,⁹ T. Sumiyoshi,⁴⁸ K. Suzuki,⁹ S. Suzuki,⁵⁴

S. Y. Suzuki,⁹ S. K. Swain,⁸ K. Takahashi,⁴⁷ F. Takasaki,⁹ B. Takeshita,³² K. Tamai,⁹ Y. Tamai,³² N. Tamura,³⁰ K. Tanabe,⁴⁶ J. Tanaka,⁴⁶ M. Tanaka,⁹ G. N. Taylor,²² A. Tchouvikov,³⁵ Y. Teramoto,³¹ S. Tokuda,²³ M. Tomoto,⁹ T. Tomura,⁴⁶ S. N. Tovey,²² K. Trabelsi,⁸ T. Tsuboyama,⁹ T. Tsukamoto,⁹ K. Uchida,⁸ S. Uehara,⁹ K. Ueno,²⁷ T. Uglov,¹³ Y. Unno,³ S. Uno,⁹ N. Uozaki,⁴⁶ Y. Ushiroda,⁹ S. E. Vahsen,³⁵ G. Varner,⁸ K. E. Varvell,⁴¹ C. C. Wang,²⁷ C. H. Wang,²⁶ J. G. Wang,⁵³ M.-Z. Wang,²⁷ M. Watanabe,³⁰ Y. Watanabe,⁴⁷ L. Widhalm,¹² E. Won,¹⁶ B. D. Yabsley,⁵³ Y. Yamada,⁹ A. Yamaguchi,⁴⁵ H. Yamamoto,⁴⁵ T. Yamanaka,³² Y. Yamashita,²⁹ Y. Yamashita,⁴⁶ M. Yamauchi,⁹ H. Yanai,³⁰ Heyoung Yang,³⁹ J. Yashima,⁹ P. Yeh,²⁷ M. Yokoyama,⁴⁶ K. Yoshida,²³ Y. Yuan,¹¹ Y. Yusa,⁴⁵ H. Yuta,¹ C. C. Zhang,¹¹ J. Zhang,⁵¹ Z. P. Zhang,³⁸ Y. Zheng,⁸ V. Zhilich,² Z. M. Zhu,³⁴ T. Ziegler,³⁵ D. Žontar,^{20,14} and D. Zürcher¹⁹

(The Belle Collaboration)

¹*Aomori University, Aomori*

²*Budker Institute of Nuclear Physics, Novosibirsk*

³*Chiba University, Chiba*

⁴*Chuo University, Tokyo*

⁵*University of Cincinnati, Cincinnati, Ohio 45221*

⁶*University of Frankfurt, Frankfurt*

⁷*Gyeongsang National University, Chinju*

⁸*University of Hawaii, Honolulu, Hawaii 96822*

⁹*High Energy Accelerator Research Organization (KEK), Tsukuba*

¹⁰*Hiroshima Institute of Technology, Hiroshima*

¹¹*Institute of High Energy Physics,
Chinese Academy of Sciences, Beijing*

¹²*Institute of High Energy Physics, Vienna*

¹³*Institute for Theoretical and Experimental Physics, Moscow*

¹⁴*J. Stefan Institute, Ljubljana*

¹⁵*Kanagawa University, Yokohama*

¹⁶*Korea University, Seoul*

¹⁷*Kyoto University, Kyoto*

¹⁸*Kyungpook National University, Taegu*

¹⁹*Institut de Physique des Hautes Énergies, Université de Lausanne, Lausanne*

²⁰*University of Ljubljana, Ljubljana*

²¹*University of Maribor, Maribor*

²²*University of Melbourne, Victoria*

²³*Nagoya University, Nagoya*

²⁴*Nara Women's University, Nara*

²⁵*National Kaohsiung Normal University, Kaohsiung*

²⁶*National Lien-Ho Institute of Technology, Miao Li*

²⁷*Department of Physics, National Taiwan University, Taipei*

²⁸*H. Niewodniczanski Institute of Nuclear Physics, Krakow*

²⁹*Nihon Dental College, Niigata*

³⁰*Niigata University, Niigata*

³¹*Osaka City University, Osaka*

³²*Osaka University, Osaka*

³³Panjab University, Chandigarh
³⁴Peking University, Beijing
³⁵Princeton University, Princeton, New Jersey 08545
³⁶RIKEN BNL Research Center, Upton, New York 11973
³⁷Saga University, Saga
³⁸University of Science and Technology of China, Hefei
³⁹Seoul National University, Seoul
⁴⁰Sungkyunkwan University, Suwon
⁴¹University of Sydney, Sydney NSW
⁴²Tata Institute of Fundamental Research, Bombay
⁴³Toho University, Funabashi
⁴⁴Tohoku Gakuin University, Tagajo
⁴⁵Tohoku University, Sendai
⁴⁶Department of Physics, University of Tokyo, Tokyo
⁴⁷Tokyo Institute of Technology, Tokyo
⁴⁸Tokyo Metropolitan University, Tokyo
⁴⁹Tokyo University of Agriculture and Technology, Tokyo
⁵⁰Toyama National College of Maritime Technology, Toyama
⁵¹University of Tsukuba, Tsukuba
⁵²Utkal University, Bhubaneswar
⁵³Virginia Polytechnic Institute and State University, Blacksburg, Virginia 24061
⁵⁴Yokkaichi University, Yokkaichi
⁵⁵Yonsei University, Seoul

Abstract

We report measurements of time dependent decay rates for $B^0(\bar{B}^0) \rightarrow D^{(*)\mp}\pi^\pm$ decays and extraction of CP violation parameters containing ϕ_3 . We use a fully reconstructed $D^{(*)}\pi$ sample from a 140 fb^{-1} data sample collected at the $\Upsilon(4S)$ resonance with the Belle detector at the KEKB e^+e^- storage ring. We obtain the CP violation parameters for $D^*\pi$ and $D\pi$ decays,

$$\begin{aligned}
 2R_{D^*\pi} \sin(2\phi_1 + \phi_3 + \delta_{D^*\pi}) &= 0.092 \pm 0.059 \text{ (stat)} \pm 0.016 \text{ (syst)} \pm 0.036 \text{ } (D^*l\nu), \\
 2R_{D^*\pi} \sin(2\phi_1 + \phi_3 - \delta_{D^*\pi}) &= 0.033 \pm 0.056 \text{ (stat)} \pm 0.016 \text{ (syst)} \pm 0.036 \text{ } (D^*l\nu), \\
 2R_{D\pi} \sin(2\phi_1 + \phi_3 + \delta_{D\pi}) &= 0.094 \pm 0.053 \text{ (stat)} \pm 0.013 \text{ (syst)} \pm 0.036 \text{ } (D^*l\nu), \\
 2R_{D\pi} \sin(2\phi_1 + \phi_3 - \delta_{D\pi}) &= 0.022 \pm 0.054 \text{ (stat)} \pm 0.013 \text{ (syst)} \pm 0.036 \text{ } (D^*l\nu),
 \end{aligned}$$

where $R_{D^{(*)}\pi}$ is the ratio of the magnitudes of the doubly-Cabibbo-suppressed and Cabibbo-favoured amplitudes which contribute to the B meson decay to the final state of interest, and $\delta_{D^{(*)}\pi}$ is the strong phase difference between them. The last error, denoted $D^*l\nu$, represents the systematic error which depends on the statistics of a $D^*l\nu$ control sample.

PACS numbers:

INTRODUCTION

The good agreement between direct measurements of $\sin 2\phi_1$ [1, 2] and the outcome of global CKM fits strongly supports the standard model explanation of CP violation. To determine whether it is the complete description or whether additional factors come into play, however, must wait for further measurements of other CKM parameters. Of particular importance among them is ϕ_3 . The measurements of time-dependent decay rates of $B^0(\bar{B}^0) \rightarrow D^{(*)\mp}\pi^\pm$ provide a theoretically clean method for extracting $\sin(2\phi_1 + \phi_3)$ [3]. There are two ways for a state which is initially B^0 to be found as $D^{(*)-}\pi^+$ at a later time t . It can occur either directly through a Cabibbo-favoured decay (CFD) or through mixing followed by doubly-Cabibbo-suppressed decay (DCSD) as shown in Fig. 1. The DCSD contains V_{ub} and its phase ϕ_3 shows up in the interference term.

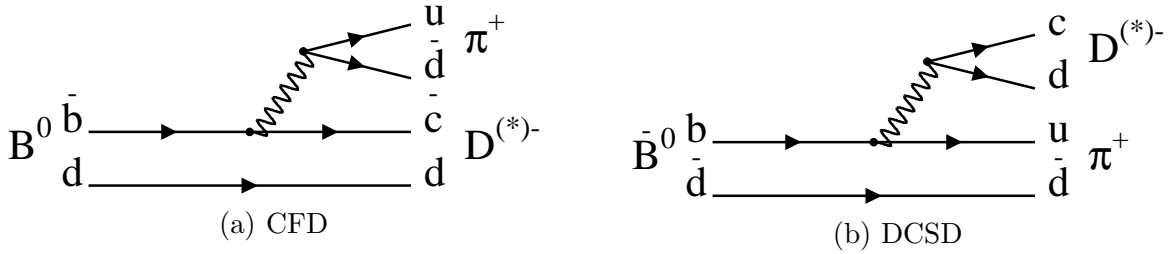


FIG. 1: Contributions to $B^0 \rightarrow D^{(*)-}\pi^+$ can come either (a) from CFD or (b) from mixing followed by DCSD.

These processes contain only tree diagrams and there is no theoretical ambiguity such as tree-penguin interference.

The time-dependent decay rates are given by [4]

$$\begin{aligned}\Gamma(B^0 \rightarrow D^{(*)+}\pi^-) &\propto \frac{1}{2\tau_{B^0}} e^{-t/\tau_{B^0}} \left[1 - C \cos \Delta m t - (-1)^L S^+ \sin \Delta m t \right], \\ \Gamma(B^0 \rightarrow D^{(*)-}\pi^+) &\propto \frac{1}{2\tau_{B^0}} e^{-t/\tau_{B^0}} \left[1 + C \cos \Delta m t - (-1)^L S^- \sin \Delta m t \right], \\ \Gamma(\bar{B}^0 \rightarrow D^{(*)+}\pi^-) &\propto \frac{1}{2\tau_{B^0}} e^{-t/\tau_{B^0}} \left[1 + C \cos \Delta m t + (-1)^L S^+ \sin \Delta m t \right], \\ \Gamma(\bar{B}^0 \rightarrow D^{(*)-}\pi^+) &\propto \frac{1}{2\tau_{B^0}} e^{-t/\tau_{B^0}} \left[1 - C \cos \Delta m t + (-1)^L S^- \sin \Delta m t \right],\end{aligned}$$

where τ_{B^0} is the B^0 lifetime, Δm is the $B^0 - \bar{B}^0$ mixing parameter, $C = (1 - R^2) / (1 + R^2)$, R is the ratio of the magnitudes of the DCSD and CFD amplitudes (we assume the magnitudes of both the CFD and DCSD amplitudes are the same for B^0 and \bar{B}^0 decays), $S^\pm = 2R \sin(2\phi_1 + \phi_3 \pm \delta)$, δ is the strong phase difference between DCSD and CFD, and L is the orbital angular momentum of the final state (1 for $D^*\pi$ and 0 for $D\pi$). R and δ , and hence S^\pm , are not necessarily the same for $D^*\pi$ and $D\pi$ final states, and are denoted with subscripts, $D^*\pi$ and $D\pi$, in what follows. We neglect terms of $\mathcal{O}(R^2)$, and hence take $C = 1$. CP violation appears as non-zero values of S^\pm .

In order to extract $\sin(2\phi_1 + \phi_3)$ from these distributions it is necessary to have some external input on at least one of R and δ . Several methods have been proposed to measure R [3], which is predicted to be about 0.02 [5], using information from $B^0 \rightarrow D_s^{(*)+}\pi^-$ or

$B^+ \rightarrow D^{(*)+}\pi^0$. Of these modes only $B^0 \rightarrow D_s^+\pi^-$ has been observed [6, 7], and the theoretical uncertainties involved in extracting R are unclear. Therefore, in this analysis we do not attempt to extract $\sin(2\phi_1 + \phi_3)$, and simply measure S^\pm .

THE BELLE EXPERIMENT AND DATASET

The KEKB e^+e^- collider [8] is a pair of asymmetric-energy electron storage rings with 8.0 GeV e^- and 3.5 GeV e^+ , that operates in the center-of-mass (CM) energy region around the $\Upsilon(4S)$ resonance, $\sqrt{s} = 10.58$ GeV. For this analysis, we use a 140 fb^{-1} data sample collected with the Belle detector that contains 152 million $B\bar{B}$ events.

The Belle detector is a large-solid-angle magnetic spectrometer that consists of a three-layer silicon vertex detector (SVD), a 50-layer central drift chamber (CDC), an array of aerogel threshold Čerenkov counters (ACC), a barrel-like arrangement of time-of-flight scintillation counters (TOF), and an electromagnetic calorimeter comprised of CsI(Tl) crystals (ECL) located inside a superconducting solenoid coil that provides a 1.5 T magnetic field. An iron flux-return located outside of the coil is instrumented to detect K_L^0 mesons and to identify muons (KLM). The detector is described in detail elsewhere [9].

EVENT RECONSTRUCTION

We select hadronic $B\bar{B}$ events requiring that the event has, i) at least five tracks, ii) an event vertex with radial and z coordinates within 1.5 cm and 3.5 cm respectively of the detector origin, iii) a total reconstructed CM energy greater than $0.5W$ (W is the $\Upsilon(4S)$ CM energy), iv) a z component of the net reconstructed CM momentum less than $0.3W/c$, v) a total energy deposited to ECL between $0.025W$ and $0.9W$. For the $B \rightarrow D^{*+}\pi^-$ event selection, we use the decay chain of $D^{*+} \rightarrow D^0\pi^+$, and $D^0 \rightarrow K^-\pi^+$, $K^-\pi^+\pi^0$, $K^-\pi^+\pi^+\pi^-$ (charge conjugate modes are implied in this section.) For the $B \rightarrow D^+\pi^-$ event selection, we use $D^+ \rightarrow K^-\pi^+\pi^+$ decays. Charged tracks are required to have minimum of one hit (two hits) in the $r\text{-}\phi$ (z) plane of the SVD in order to allow precise vertex determination. To separate kaons from pions, we form a likelihood for each track, $\mathcal{L}_{K(\pi)}$, that is derived from the CDC dE/dx measurements and the responses from the ACC and the TOF. The kaon likelihood ratio, $P(K/\pi) = \mathcal{L}_K/(\mathcal{L}_K + \mathcal{L}_\pi)$, has values between 0 (likely to be a pion) and 1 (likely to be a kaon). We require charged kaons to satisfy $P(K/\pi) > 0.3$. No such requirement is imposed to select charged pions coming from D decays.

For D^0 selection, we require the invariant mass of the daughter particles to be within $\pm 16.5 \text{ MeV}/c^2$, $\pm 24.0 \text{ MeV}/c^2$, $\pm 13.5 \text{ MeV}/c^2$ of the nominal D^0 mass, for $K^-\pi^+$, $K^-\pi^+\pi^0$, $K^-\pi^+\pi^+\pi^-$ modes respectively, corresponding to $\pm 3\sigma$, where σ is the Monte Carlo determined invariant mass resolution. For the D^+ , we require the invariant mass of the daughter particles to be within $\pm 12.5 \text{ MeV}/c^2$ of the nominal D^+ mass. We use a mass- and vertex-constrained fit for D^0 and a vertex-constrained fit for D^+ . For the $D^0 \rightarrow K^-\pi^+\pi^0$ reconstruction, we further require the π^0 momentum to be greater than 200 MeV/c in the $\Upsilon(4S)$ rest frame. In this mode we also require the ratio of second to zeroth Fox-Wolfram moments [10] R_2 to be less than 0.55. We require $R_2 < 0.5$ for $D^+ \rightarrow K^-\pi^+\pi^+$.

For D^{*+} reconstruction, we combine D^0 candidates with a slow π^+ . Here slow pions are required to have momentum less than 300 MeV/c in the $\Upsilon(4S)$ rest frame. The D^* candidates are required to have the mass difference $\Delta M \equiv M_{D^0\pi} - M_{D^0}$ within $\pm 7 \text{ MeV}/c^2$,

± 2 MeV/ c^2 , ± 4 MeV/ c^2 for the $K^-\pi^+$, $K^-\pi^+\pi^0$, $K^-\pi^+\pi^+\pi^-$ modes respectively.

We reconstruct B candidates by combining the $D^{(*)+}$ candidate with a π^- candidate satisfying $P(K/\pi) < 0.8$. We identify B decays based on requirements on the energy difference $\Delta E \equiv \sum_i E_i - E_{\text{beam}}$ and the beam-energy constrained mass $M_{\text{bc}} = \sqrt{E_{\text{beam}}^2 - (\sum_i \vec{p}_i)^2}$, where E_{beam} is the beam energy in the $\Upsilon(4S)$ rest frame, and \vec{p}_i and E_i represent the momenta and energies of the daughters of the reconstructed B meson candidate. If more than one B candidates are found in the same event, we select the one with the smallest χ^2 of the vertex fit. For $D^*\pi$, we include in the χ^2 the difference between ΔM and its nominal value, divided by its resolution. We define a rectangular signal region in the ΔE - M_{bc} plane of $5.27 \text{ GeV}/c^2 < M_{\text{bc}} < 5.29 \text{ GeV}/c^2$ and $|\Delta E| < 0.045 \text{ GeV}$, corresponding to about $\pm 3\sigma$ of both quantities. For the determination of background parameters, we use events which satisfy either $M_{\text{bc}} > 5.2 \text{ GeV}/c^2$ or $-0.14 \text{ GeV} < |\Delta E| < 0.20 \text{ GeV}$, excluding the signal region. The lower bound on ΔE is chosen in order to exclude background from other B decays. We obtain signal fractions by performing an unbinned two-dimensional fit of ΔE and M_{bc} . The signal probability density function (PDF) is the product of single Gaussians in both ΔE and M_{bc} ; that for the background, which is dominated by continuum $e^+e^- \rightarrow q\bar{q}$ ($q = u, d, s, c$) processes, is the product of a first order polynomial in ΔE and an ARGUS function [11] in M_{bc} . All parameters are allowed to float in the fit, except for the kinematic limit of the ARGUS function which is fixed at the beam energy. The ΔE and M_{bc} distributions for $D^*\pi$ and $D\pi$ candidates are shown in Fig. 2. Table I summarizes the yields and purity of the events in the signal region.

TABLE I: Yields and purities of the events in the signal region.

Decay mode	Candidates	Purity
$B^0(\bar{B}^0) \rightarrow D^*\pi$	7556	95%
$B^0(\bar{B}^0) \rightarrow D\pi$	8375	88%

FLAVOUR TAGGING

We use the same flavour tagging algorithm used in our other time dependent analyses [1]. Charged leptons, pions, and kaons that are not associated with the reconstructed $D^{(*)}\pi$ decays are used to identify the flavour of the accompanying B meson (flavour tagging). The flavour determination is first performed at the level of particle tracks. We use high momentum leptons from $b \rightarrow c\ell^-\bar{\nu}$, low momentum leptons from $b \rightarrow c \rightarrow s\ell^+\nu$, charged kaons and Λ baryons from $b \rightarrow c \rightarrow s$, high momentum pions originated from $\bar{B}^0(b\bar{d}) \rightarrow D^{(*)+}X$ where $X = \pi^-, \rho^-, a_1^-, \dots$, and slow pions from $D^{*+} \rightarrow D^0\pi^+$. We use Monte Carlo simulations to determine a category-dependent variable that indicates whether a track originates from a B^0 or \bar{B}^0 . The values of this variable ranges from -1 for a reliably identified \bar{B}^0 to +1 for a reliably identified B^0 , and depend on the track's charge, CM momentum, polar angle, particle-identification probability, as well as on other kinematic variables and event-shape variables.

The results are then examined for the correlations among the track level analyses and obtain the result and quality of the flavour tagging, that are given by two parameters, q and r . $q = +1$ indicates \bar{b} hence B^0 , and $q = -1$ indicates b hence \bar{B}^0 . The parameter r is an event-by-event dilution factor ranging from $r = 0$ for no flavour discrimination to

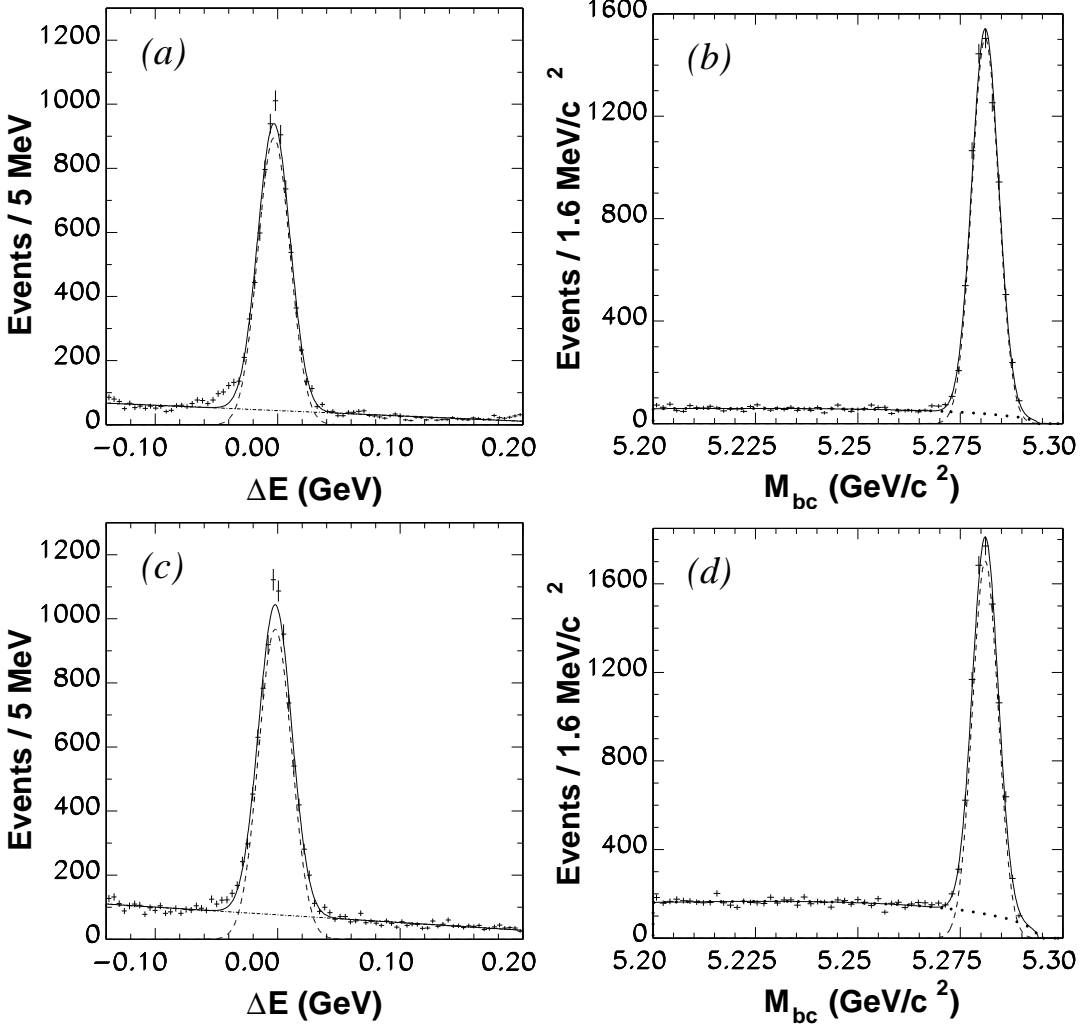


FIG. 2: (a) ΔE and (b) M_{bc} distributions for the $D^*\pi$ candidate events; (c) ΔE and (d) M_{bc} distributions for the $D\pi$ candidate events.

$r = 1$ for unambiguous flavour assignment. It is used only to sort data into six intervals of r (boundaries at 0.25, 0.5, 0.625, 0.75, 0.875), according to quality of flavour tagging. More than 99.5% of the events are assigned non-zero values of r .

VERTEX DETERMINATION

We use the same vertexing technique used in our other time dependent analyses [1]. The decay point of the reconstructed $B \rightarrow D^{(*)}\pi$ is obtained from the vertex position and momentum vector of the reconstructed D meson and π . We do not use the slow π from D^* decay, since it is poorly measured due to multiple scattering. For the decay vertex of the tagging B meson, we try to use all tracks that are not associated with the $B \rightarrow D^{(*)}\pi$ decay except those that are poorly reconstructed with a longitudinal position error in excess of 500 μm , and those which are considered likely to come from K_S^0 decay, as when combined with an oppositely charged track, form a vertex which deviates by more than 500 μm from

the B meson vertex in the r - ϕ plane.

The quality of each fitted vertex is assessed only in the z direction using the variable

$$\xi \equiv (1/2n) \sum_i^n \left[(z_{\text{after}}^i - z_{\text{before}}^i) / \epsilon_{\text{before}}^i \right]^2, \quad (1)$$

where n is the number of tracks used in the fit, z_{before}^i and z_{after}^i are the z positions of each track (at the closest approach to the origin) before and after the vertex fit, respectively, and $\epsilon_{\text{before}}^i$ is the error of z_{before}^i . A Monte Carlo study shows that ξ does not depend on the B decay length. We require $\xi < 100$ to eliminate poorly reconstructed vertices. About 3% of the fully reconstructed $D^{(*)}\pi$ vertices and 1% of the tagging B decay vertices are rejected. The proper-time difference between the fully reconstructed and associated B decay, $\Delta t \equiv t_{\text{rec}} - t_{\text{tag}}$, is calculated as $\Delta t = (z_{\text{rec}} - z_{\text{tag}})/c\beta\gamma$, where z_{rec} and z_{tag} are the z coordinates of the two B decay vertices and $\beta\gamma = 0.425$ is the Lorentz boost factor at KEKB. We reject a small fraction ($\sim 0.2\%$) of the events by requiring $|\Delta t| < 70$ ps ($\sim 45\tau_{B^0}$).

FIT PROCEDURE

Unbinned maximum likelihood fits to the four time-dependent decay rates of $D^{(*)}\pi$ are performed to extract $2R \sin(2\phi_1 + \phi_3 \pm \delta)$. We minimize $-2 \ln L = -2 \sum_i \ln L_i$ where the likelihood for the i -th event is given by

$$L_i = (1 - f_{\text{ol}}) [f_{\text{sig}} P_{\text{sig}} \otimes R_{\text{sig}} + (1 - f_{\text{sig}}) P_{\text{bkg}} \otimes R_{\text{bkg}}] + f_{\text{ol}} P_{\text{ol}} \quad (2)$$

where f_{sig} is the signal fraction and is determined from the $(\Delta E, M_{\text{bc}})$ value of each event. A small number of candidate events have large Δt values. We account for the contributions from these ‘‘outliers’’ by adding a Gaussian component P_{ol} with a width and fraction determined from the B lifetime analysis. We assume f_{ol} to be the same for signal and background. The Δt resolution, denoted by R_{sig} and R_{bkg} for the signal and background, is determined on an event-by-event basis, using the estimated uncertainties on the z vertex positions that are determined from the vertex fit. A detailed description of the resolution parameterization can be found in Ref. [12].

The PDFs for the four categories of signal events are given by

$$P_{\text{sig}}(\Delta t) = \frac{1}{4\tau_{B^0}} e^{-\Delta t/\tau_{B^0}} \left[1 \pm (1 - 2w) \cos(\Delta m \Delta t) \pm (-1)^L (1 - 2w) S^\pm \sin(\Delta m \Delta t) \right] \quad (3)$$

where the four categories, $B^0 \rightarrow D^{(*)+}\pi^-$, $B^0 \rightarrow D^{(*)-}\pi^+$, $\bar{B}^0 \rightarrow D^{(*)+}\pi^-$, $\bar{B}^0 \rightarrow D^{(*)-}\pi^+$, are represented by the sign combinations $(-, -, +)$, $(+, -, -)$, $(+, +, +)$ and $(-, +, -)$, respectively. B candidates are assigned as B^0 or \bar{B}^0 based on the value of q from the flavour tagging algorithm, and the wrong tag fractions w are determined separately in each interval of r . We define the term opposite flavour (OF) to indicate $B^0 \rightarrow D^{(*)-}\pi^+$ and $\bar{B}^0 \rightarrow D^{(*)+}\pi^-$, and same flavour (SF) to indicate $\bar{B}^0 \rightarrow D^{(*)-}\pi^+$ and $B^0 \rightarrow D^{(*)+}\pi^-$.

The background PDF is parameterized as a sum of a δ -function component and an exponential component with a lifetime τ_{bkg} .

$$P_{\text{bkg}} = f_{\text{bkg}}^\delta \delta(\Delta t - \mu_{\text{bkg}}^\delta) + \frac{(1 - f_{\text{bkg}}^\delta)}{2\tau_{\text{bkg}}} e^{-|\Delta t - \mu_{\text{bkg}}^\tau|/\tau_{\text{bkg}}}, \quad (4)$$

where f_{bkg}^δ is the fraction of events contained in the δ -function, and μ_{bkg}^δ and μ_{bkg}^τ are the mean values of $|\Delta t|$ in the δ -function and exponential components, respectively. The resolution function is parameterized as a sum of two Gaussians. Different parameter values are used for $R_{\text{bkg}}(\Delta t)$ depending on whether or not both vertices are reconstructed with multiple tracks. These parameters are determined from the sideband region described above.

EXTRactions OF B MESON LIFETIME AND $B\bar{B}$ MIXING

To test the procedures of Δt determination and flavour tagging, we extract the lifetime of the neutral B meson, τ_{B^0} , and the $B^0 - \bar{B}^0$ mixing parameter Δm . When all four signal categories are combined, the signal PDF reduces to an exponential lifetime distribution. The Δt distributions for the $D^*\pi$ and $D\pi$ data samples and fit results are shown in Fig. 3. We obtain $\tau_{B^0} = 1.598 \pm 0.040$ ps for the $D^*\pi$ sample and $\tau_{B^0} = 1.594 \pm 0.033$ ps for the $D\pi$ sample, respectively. These values are in good agreement with the world average (1.542 ± 0.016 ps) [13].

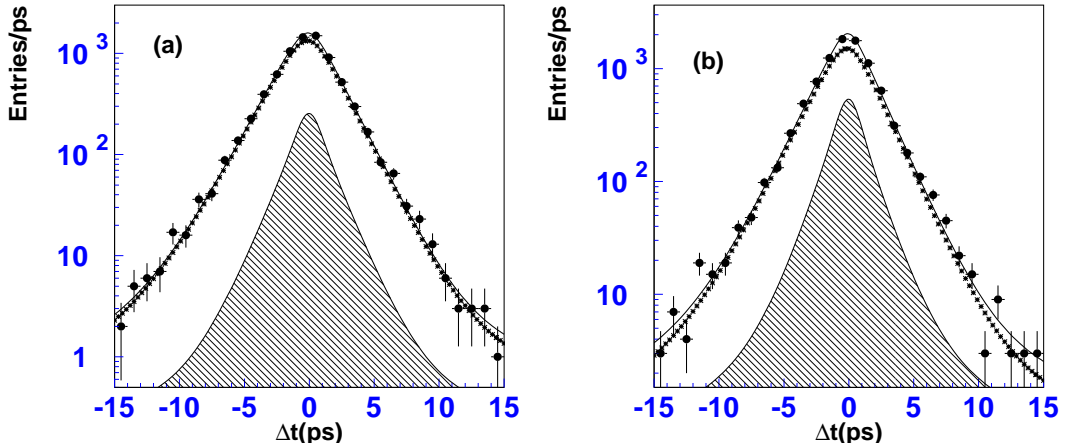


FIG. 3: Δt distributions for all four categories of signal events combined for (a) $D^*\pi$ and (b) $D\pi$. Results of lifetime fits are shown by solid lines (total), dotted lines (signal part), and hatched areas (background part), respectively.

Combining the two OF modes and the two SF modes and ignoring the CP violating sin-like terms (which cancel if $\delta = 0$, and are in any case small), the asymmetry ($OF - SF$)/($OF + SF$) behaves as $(1 - 2w) \cos(\Delta m \Delta t)$. The asymmetry distributions for $D^*\pi$ and $D\pi$ data samples and fit results are shown in Fig. 4. We obtain $\Delta m = 0.501 \pm 0.017$ ps⁻¹ for the $D^*\pi$ sample and $\Delta m = 0.488 \pm 0.018$ ps⁻¹ for the $D\pi$ sample, respectively. These values are also in good agreement with the world average (0.489 ± 0.008 ps⁻¹) [13]. We also obtain wrong tag fractions for each interval of r , which we denote by w_i ($i = 1, 2, 3, 4, 5, 6$), for both $D^*\pi$ and $D\pi$ data samples from these fits. They are used in the next step.

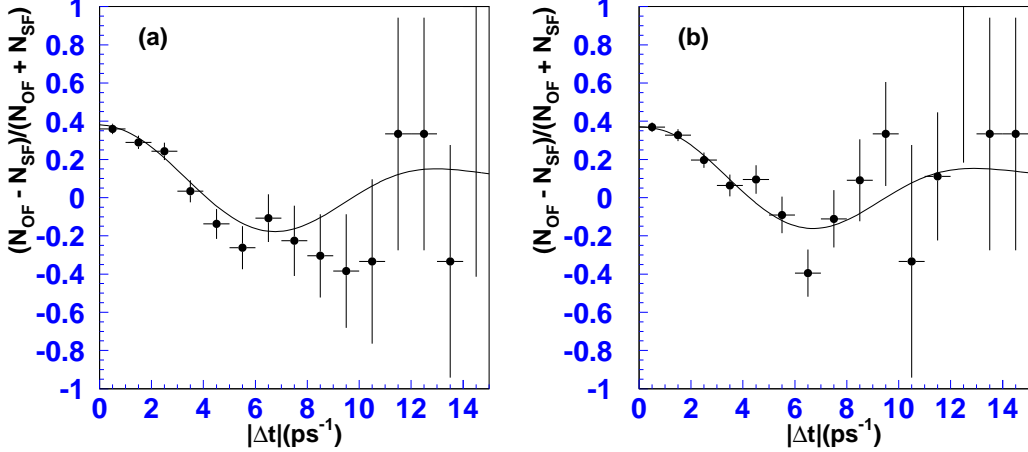


FIG. 4: (OF-SF)/(OF+SF) asymmetry distributions for B^0 and \bar{B}^0 tagged events combined for (a) $D^*\pi$ and (b) $D\pi$. Results of mixing fits are shown in solid lines.

EXTRACTION OF $2R \sin(2\phi_1 + \phi_3 \pm \delta)$

The Δt distributions for the four signal categories with fit results are shown in Fig. 5 for the $D^*\pi$ and in Fig. 6 for the $D\pi$ samples, respectively. The fit results are given in Table II.

TABLE II: Fit results for $2R \sin(2\phi_1 + \phi_3 \pm \delta)$.

Decay Mode	S^+	S^-
$B \rightarrow D^*\pi$	0.092 ± 0.059	0.033 ± 0.056
$B \rightarrow D\pi$	0.094 ± 0.053	0.022 ± 0.054

Δt distributions for the subsamples of events with the best quality flavour tagging ($0.875 < r < 1.000$) are shown in Fig. 7 for the $D^*\pi$ and in Fig. 8 for the $D\pi$ samples, respectively. Fit results from the entire r region are shown in solid lines. Since the dilution due to mistagging is small for these subsamples, the presence of sin-like modulations can be seen more easily. Their effect is more pronounced in the same flavour distributions, since the total event rate is smaller.

The presence of CP violation can be visually examined by defining the asymmetries between OF events, and between SF events.

$$A_{\text{OF}} \equiv \frac{\Gamma(\bar{B}^0 \rightarrow D^{(*)+}\pi^-) - \Gamma(B^0 \rightarrow D^{(*)-}\pi^+)}{\Gamma(\bar{B}^0 \rightarrow D^{(*)+}\pi^-) + \Gamma(B^0 \rightarrow D^{(*)-}\pi^+)} \quad (5)$$

$$A_{\text{SF}} \equiv \frac{\Gamma(\bar{B}^0 \rightarrow D^{(*)-}\pi^+) - \Gamma(B^0 \rightarrow D^{(*)+}\pi^-)}{\Gamma(\bar{B}^0 \rightarrow D^{(*)-}\pi^+) + \Gamma(B^0 \rightarrow D^{(*)+}\pi^-)}. \quad (6)$$

In the case that $\delta = 0$, they reduce to $A_{\text{OF}} \propto (-1)^L 2R \sin(2\phi_1 + \phi_3) \sin(\Delta m \Delta t) / (1 + \cos(\Delta m \Delta t))$ and $A_{\text{SF}} \propto (-1)^L 2R \sin(2\phi_1 + \phi_3) \sin(\Delta m \Delta t) / (1 - \cos(\Delta m \Delta t))$, respectively.

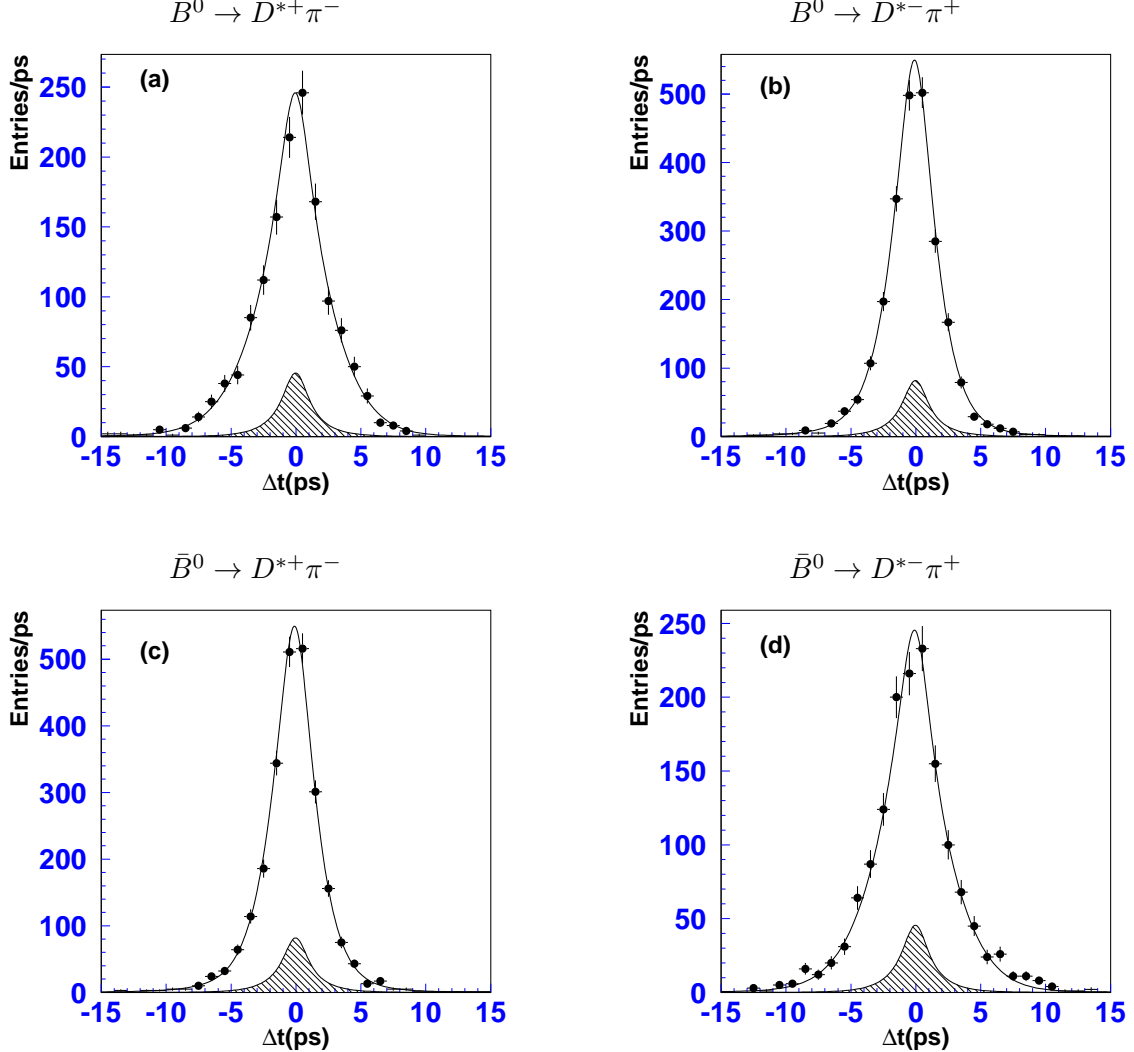


FIG. 5: Δt distributions for the $D^*\pi$ final states. (a) $B^0 \rightarrow D^{*+}\pi^-$, (b) $B^0 \rightarrow D^{*-}\pi^+$, (c) $\bar{B}^0 \rightarrow D^{*+}\pi^-$, (d) $\bar{B}^0 \rightarrow D^{*-}\pi^+$. Curves are the fit results. Hatched regions are the backgrounds.

This indicates that CP violation can be observed as sin-like oscillations in these asymmetries. They are shown in Fig. 9.

SYSTEMATIC ERRORS

The systematic errors in this analysis come from i) the uncertainties of parameters which are constrained in the fit, including Δt resolution function parameters, background shapes and fractions, wrong tag fractions and physics parameters; ii) possible asymmetries in the flavour tagging due to the presence of CP violation in the tagging side [14], iii) biases in the fit induced by our vertexing or fitting procedures, or by detector misalignment.

For item i), we repeat the fits varying each parameter value by $\pm 1\sigma$ and assign the larger difference of S^\pm from their values in the default fit as the error. In addition, we

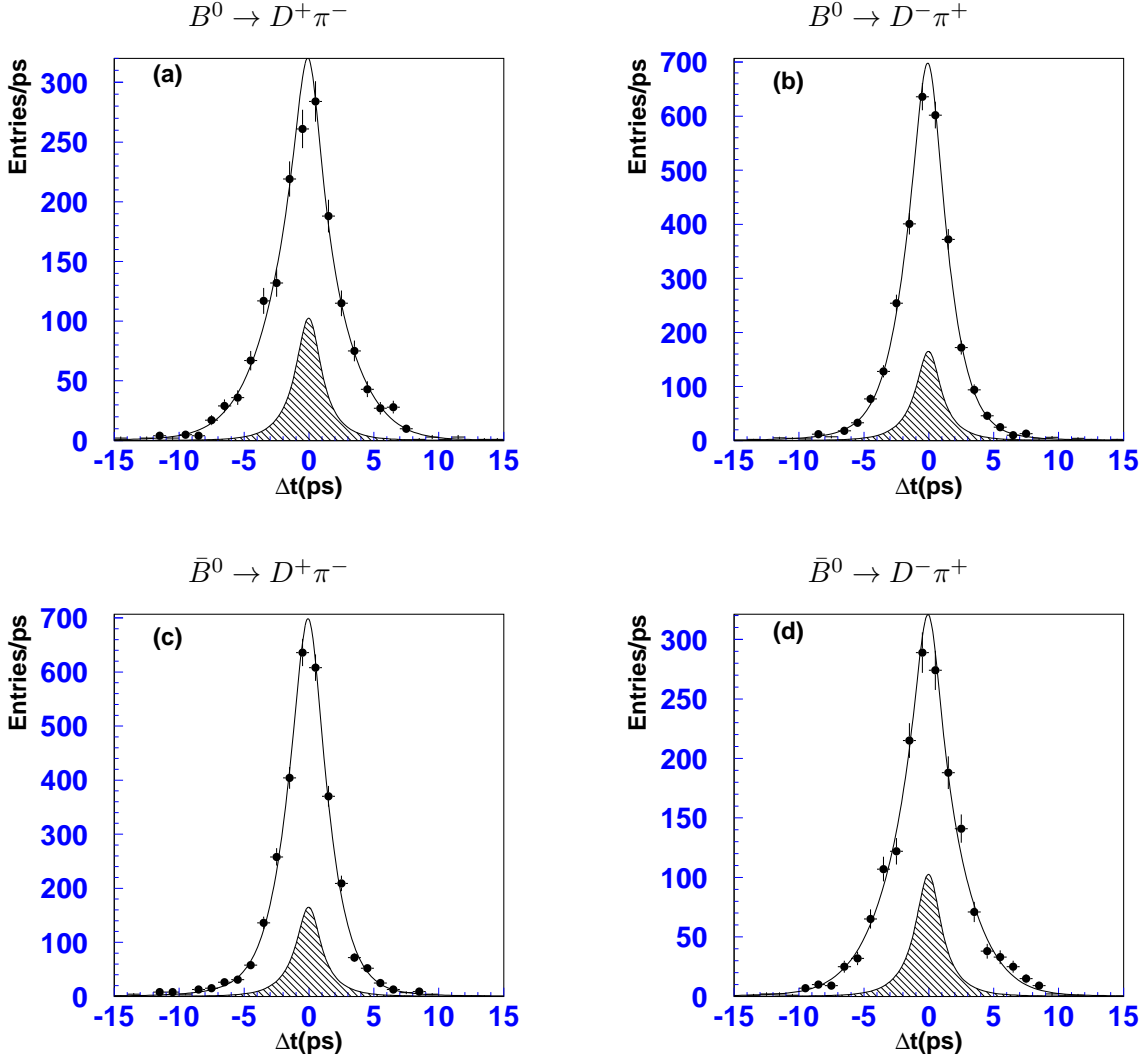


FIG. 6: Δt distributions for the $D\pi$ final states. (a) $B^0 \rightarrow D^+\pi^-$, (b) $B^0 \rightarrow D^-\pi^+$, (c) $\bar{B}^0 \rightarrow D^+\pi^-$, (d) $\bar{B}^0 \rightarrow D^-\pi^+$. Curves are the fit results. Hatched regions are the backgrounds.

test the vertexing procedure by varying the selection requirement on ξ by ± 50 , and assign a corresponding error. We also repeated the fit varying the requirement on Δt , and find negligible changes in the results.

To estimate items ii) and iii), we use a $B^0 \rightarrow D^*\ell\nu$ control sample [15], with identical procedures for the Δt determination and flavour tagging. The $D^*\ell\nu$ decay is flavour-specific and should show no time-dependent CP violating asymmetry unless there is asymmetry in the tagging side, or unless an asymmetry is induced by some bias. Whilst the tagging side should have no asymmetry if primary leptons are used for the flavour tagging, it is possible to introduce a small asymmetry when daughter particles of hadronic decays such as $D^{(*)}\pi$ are used in the flavour tagging procedure, due to the same CP violating effect which is the subject of this paper. We fit the $D^*\ell\nu$ control sample and obtain $S_{D^*\ell\nu}^+ = 0.017 \pm 0.018$ & $S_{D^*\ell\nu}^- = -0.019 \pm 0.017$. We do not observe any significant deviation from zero. In order

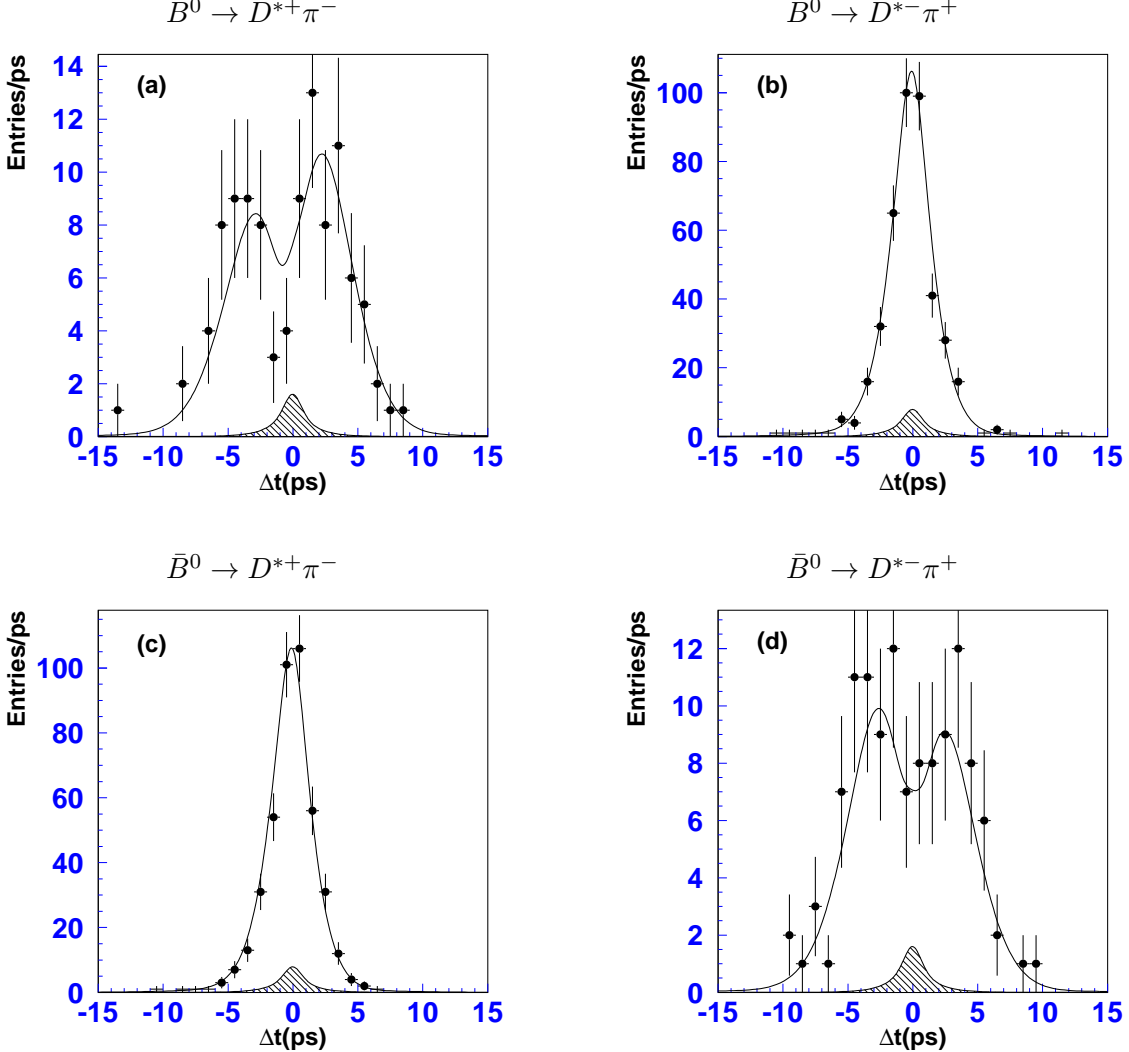


FIG. 7: Δt distributions for the $D^*\pi$ data in the $0.875 < r < 1.000$ flavour tagging quality bin. (a) $B^0 \rightarrow D^{*+}\pi^-$, (b) $B^0 \rightarrow D^{*-}\pi^+$, (c) $\bar{B}^0 \rightarrow D^{*+}\pi^-$, (d) $\bar{B}^0 \rightarrow D^{*-}\pi^+$. Curves are the fit results. Hatched regions are the backgrounds.

to take a conservative estimate of the systematic error, we assign the maximum value of the central values $\pm 1\sigma$, 0.036, as the systematic error due to possible fit biases. This is the dominant source of systematic error in this analysis. Since its size is determined by the size of the $D^*l\nu$ control sample, it will naturally decrease as the accumulated luminosity increases.

We also perform a number of other cross-checks of our fitting procedure. We repeat the entire analysis on a large, generic Monte Carlo sample, and obtain values for the lifetime, mixing and CP violation parameters which are consistent with expectation for both $D\pi$ and $D^*\pi$. We also perform the fit on signal $D^*\pi$ Monte Carlo samples generated with different values of $R_{D^*\pi}$, $\delta_{D^*\pi}$ and $\sin(2\phi_1 + \phi_3)$; in each case the results of the fit are consistent with the input values within the statistical error, which in each case is smaller than that of the

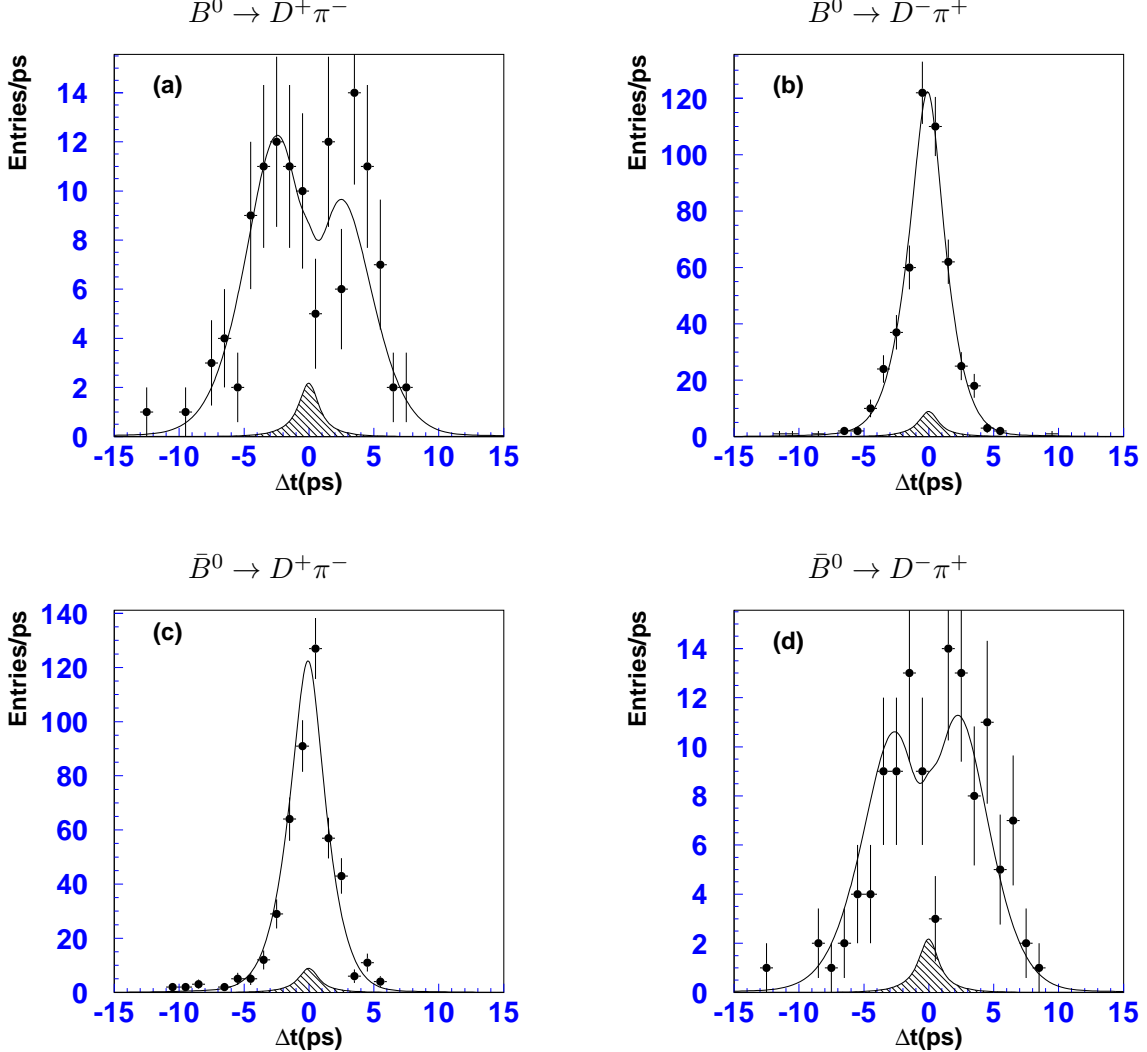


FIG. 8: Δt distributions for the $D\pi$ events in the $0.875 < r < 1.000$ flavour tagging quality bin. (a) $B^0 \rightarrow D^+ \pi^-$, (b) $B^0 \rightarrow D^- \pi^+$, (c) $\bar{B}^0 \rightarrow D^+ \pi^-$, (d) $\bar{B}^0 \rightarrow D^- \pi^+$. Curves are the fit results. Hatched regions are the backgrounds.

$D^*l\nu$ control sample.

Table III summarizes the systematic errors.

CONCLUSION

We obtain

$$\begin{aligned}
 2R_{D^*\pi} \sin(2\phi_1 + \phi_3 + \delta_{D^*\pi}) &= 0.092 \pm 0.059 \text{ (stat)} \pm 0.016 \text{ (syst)} \pm 0.036 \text{ ($D^*l\nu$)}, \\
 2R_{D^*\pi} \sin(2\phi_1 + \phi_3 - \delta_{D^*\pi}) &= 0.033 \pm 0.056 \text{ (stat)} \pm 0.016 \text{ (syst)} \pm 0.036 \text{ ($D^*l\nu$)}, \\
 2R_{D\pi} \sin(2\phi_1 + \phi_3 + \delta_{D\pi}) &= 0.094 \pm 0.053 \text{ (stat)} \pm 0.013 \text{ (syst)} \pm 0.036 \text{ ($D^*l\nu$)}, \\
 2R_{D\pi} \sin(2\phi_1 + \phi_3 - \delta_{D\pi}) &= 0.022 \pm 0.054 \text{ (stat)} \pm 0.013 \text{ (syst)} \pm 0.036 \text{ ($D^*l\nu$)}.
 \end{aligned}$$

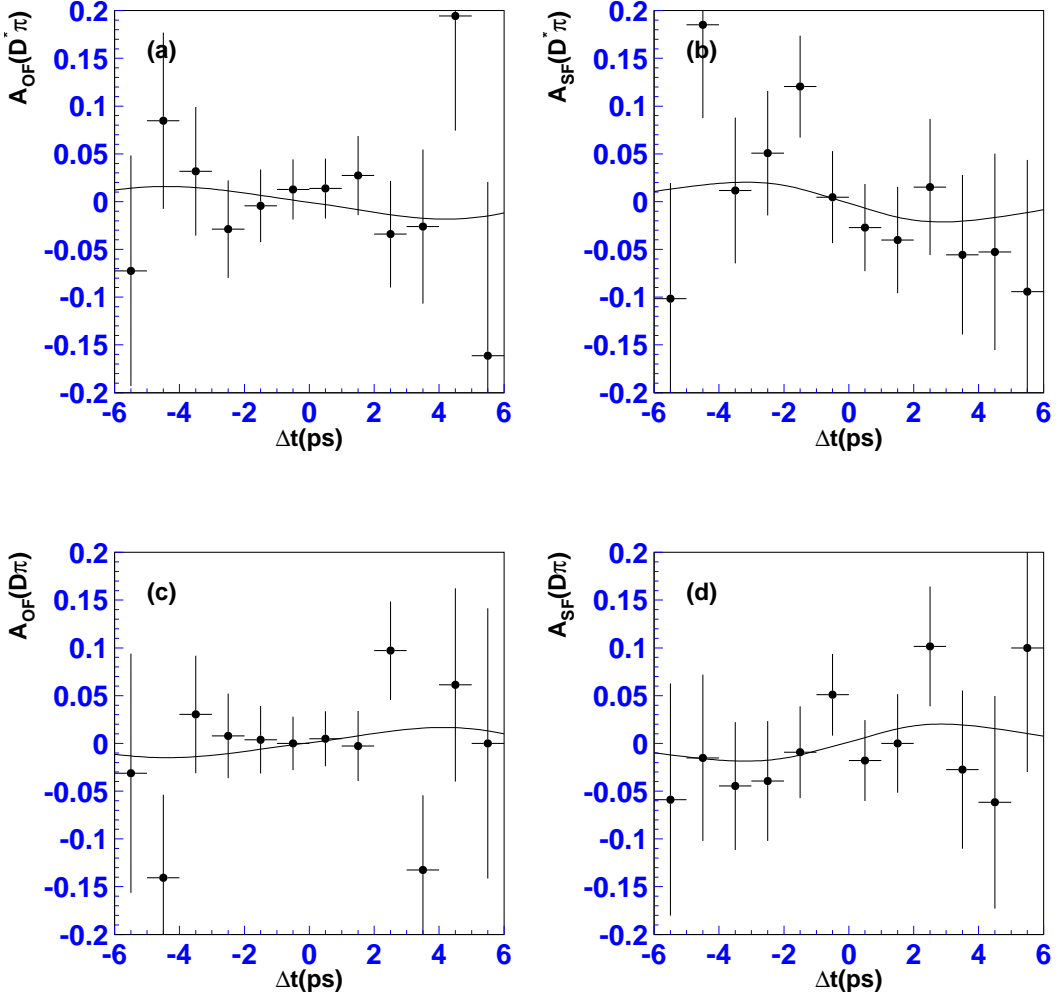


FIG. 9: Asymmetries (a) $A_{OF}(D^*\pi)$, (b) $A_{SF}(D^*\pi)$, (c) $A_{OF}(D\pi)$, (d) $A_{SF}(D\pi)$. The whole range of r is used. Curves are the fit results.

We have separated the systematic error related to the size of the $D^*l\nu$ control sample from the other systematics. The statistical error is too large to make any inference regarding ϕ_3 . Reduction of the error with more statistics, and improvement in the knowledge regarding the values of $R_{D^{(*)}\pi}$, will allow $\sin(2\phi_1 + \phi_3)$ to be extracted using this technique in future.

Acknowledgements

We wish to thank the KEKB accelerator group for the excellent operation of the KEKB accelerator. We acknowledge support from the Ministry of Education, Culture, Sports, Science, and Technology of Japan and the Japan Society for the Promotion of Science; the Australian Research Council and the Australian Department of Industry, Science and Resources; the National Science Foundation of China under contract No. 10175071; the Department of Science and Technology of India; the BK21 program of the Ministry of Education of Korea and the CHEP SRC program of the Korea Science and Engineering

TABLE III: Systematic errors in the $2R \sin(2\phi_1 + \phi_3 \pm \delta)$ extractions.

Sources	$\Delta(2R_{D^*\pi} \sin(2\phi_1 + \phi_3 \pm \delta_{D^*\pi}))$	$\Delta(2R_{D\pi} \sin(2\phi_1 + \phi_3 \pm \delta_{D\pi}))$
Signal Δt resolution	0.014	0.010
Background Δt shape	0.001	0.003
Background fraction	0.002	0.001
Wrong tag fraction	0.006	0.006
Vertexing	0.005	0.005
Physics parameters ($\Delta m, \tau_{B^0}$)	0.001	0.002
Combined	0.016	0.013
$D^*l\nu$ sample	0.036	0.036

Foundation; the Polish State Committee for Scientific Research under contract No. 2P03B 17017; the Ministry of Science and Technology of the Russian Federation; the Ministry of Education, Science and Sport of the Republic of Slovenia; the National Science Council and the Ministry of Education of Taiwan; and the U.S. Department of Energy.

^{*} on leave from Fermi National Accelerator Laboratory, Batavia, Illinois 60510

[†] on leave from University of Pittsburgh, Pittsburgh PA 15260

[‡] on leave from Nova Gorica Polytechnic, Nova Gorica

- [1] K. Abe *et al.* (Belle Collaboration), Phys. Rev. D **66** (2002) 071102(R).
- [2] B. Aubert *et al.* (BaBar Collaboration), Phys. Rev. Lett. **89** (2002) 201802.
- [3] I. Dunietz and R.G. Sachs, Phys. Rev. D **37** (1988) 3186, *Erratum*: Phys. Rev. D **39** (1989) 3515; I. Dunietz, Phys. Lett. B **427** (1998) 179.
- [4] R. Fleischer, [hep-ph/0304027](#).
- [5] D.A. Suprun, C.-W. Chiang and J.L. Rosner, Phys. Rev. D **65** (2002) 054025.
- [6] P. Krovovny *et al.* (Belle Collaboration), Phys. Rev. Lett. **89** (2002) 231804.
- [7] B. Aubert *et al.* (BaBar Collaboration), Phys. Rev. Lett. **90** (2003) 181803.
- [8] S. Kurokawa, Nucl. Instr. and Meth. A **499** (2003) 1.
- [9] A. Abashian *et al.* (Belle Collaboration), Nucl. Instr. and Meth. A **479** (2002) 117.
- [10] G.C. Fox and S. Wolfram, Phys. Rev. Lett. **41** (1978) 1581.
- [11] H. Albrecht *et al.* (ARGUS Collaboration), Phys. Lett. B **241** (1990) 278.
- [12] K. Abe, *et al.* (Belle Collaboration), Phys. Rev. Lett. **88** (2002) 171801.
- [13] K. Hagiwara *et al.* (Particle Data Group), Phys. Rev. D **66** (2002) 010001.
- [14] O. Long, M. Baak, R.N. Cahn and D. Kirkby, [hep-ex/0303030](#).
- [15] K. Hara, M. Hazumi *et al.* (Belle Collaboration), Phys. Rev. Lett. **89** (2002) 251803.